REEF DELINEATION BY OFFSET VERTICAL SEISMIC PROFILING AND SEISMIC DIFFRACTIONS

ALEXANDER KLOKOV[1], DAMIR IRKABAEV[2], TATIANA SHAROVA[2] and NAIL MUNASYPOV[3]

[1] *Bureau of Economic Geology, The University of Texas at Austin, University Station, Box X, Austin, TX 78713-8924, U.S.A. alexander.klokov@gmail.com*
[2] *SPC Geostra, 3 Luganskaya St., Ufa, Republic of Bashkortostan, 450071, Russia.*
[3] *Bashneftegeofizika, 13 Lenina St., Ufa, Republic of Bashkortostan, 450000, Russia.*

(Received October 22, 2014; accepted January 15, 2015)

ABSTRACT

Klokov, A., Irkabaev, D., Sharova, T. and Munasypov, N., 2015. Reef delineation by offset vertical seismic profiling and seismic diffractions. *Journal of Seismic Exploration*, 24: 135-150.

A reef is a geologic body that typically has irregular edges. The complex geometry of reef margins produces scattering of seismic energy that attenuates reflections and complicates reef characterization by conventional seismic attribute analysis. On the other hand, this scattering provides abundant diffraction waves that bring information about the reef.

In this paper, we extract diffractions from offset vertical seismic profiling data and use these diffractions to delineate a reef deposited in the Volga Region of Russia. First, we construct diffraction images for each acquisition azimuth that allows detection of scattering objects. Then, we locate each scatterer around the borehole by performing polarization analysis of corresponding diffraction events. The located diffractors outline the reef body. The diffraction analysis is combined with conventional instantaneous amplitude analysis.

KEY WORDS: diffraction imaging, borehole geophysics, VSP, multicomponent, shear waves, interpretation, carbonate, reef.

INTRODUCTION

Subsurface reefs can have abnormally high porosity and permeability (Chuanmao and Friedman, 1992; Adriansyah and McMechan, 2001; Verwer et al., 2008). Being capped by impermeable rock, such reefs form high-quality reservoirs and are exploration goals in geophysical prospecting.

0963-0651/15/$5.00

Positioning and characterization of these targets are not trivial (Chopra and Marfurt, 2007). Contrast in acoustic impedance between a reef and accommodating carbonate rocks is often minor, which results in subtle reflections. Because of their tendency to exhibit active growth and rapid diagenetic alterations, reefal buildups often are complex structures with irregular edges that scatter seismic energy, thereby further weakening the reflected wavefield. Diagenesis can also create internal reflectivity that complicates interpretation of reefs' images (Phipps and Roberts, 1988).

Seismic attributes significantly facilitate identification of reefal buildups. Skirius et al. (1999) applied coherency and spectral decomposition mapping techniques to interpret 3D data acquired in Alberta, Canada. The attributes provided more accurate imaging of the reef edges in comparison to amplitude slices. Marroquin et al. (2009) applied automated seismic facies classification to interpret a reef system in the Devonian Winnipegosis Formation. Russian et al. (2010) described the Horseshoe Atoll in Texas by a multi-attribute analysis of P-wave and S-wave data using variance-based coherence and volumetric curvature. The reef was better resolved in their SH volume. The PP volume, however, better delineated smaller reef structures generally defined as "patch" reefs. Saadatinejad and Sarkarinejad (2011) performed spectral decomposition to interpret the Fahliyan Formation in the southwestern part of Iran. Bueno et al. (2014) identified a reef in a Brazilian carbonate field using sweetness attribute, spectral decomposition, and facies distribution.

Seismic attribute analysis techniques often imply usage of time (or depth) slices, which allows tracking changes in the shape of the object with depth and identification of a reef by geometrical considerations. This option is not available when working with two-dimensional seismic data, and special reef detection criteria are required. Caughlin et al. (1976) located and mapped Silurian reef buildups in northern Michigan. Criteria for reef detection had been discussed: lifting and weakening of the overlying horizon and disruption of the underlying horizon. The reef appeared as a "dim spot" on seismic sections. Interpretation of reefs in the Western Canadian Sedimentary Basin was presented by Kuhme (1987). Anderson et al. (1989) delineated the Snipe Lake reef in west-central Alberta by using interference phenomena ¦ an off-reef peak that was one half-cycle and that subsided laterally when going onreef.

The discussion of 2D seismic sections may seem to be outdated; however, such discussion is up to date for borehole seismic. Vertical seismic profiling (VSP), when receivers are stationed in a drilled well (Hardage, 2000), and crosswell seismic survey, when both receivers and sources are located in a well (Antonelli et al., 2004), provide data with higher signal power and higher frequency content. Hence, borehole seismic favors identification, delineation, and characterization of subtle reefal bodies. Dupal and Miller (1985) studied the potential of multi-offset VSP for the delineation of reefs in western Michigan.

The migrated data revealed reflection corresponding to the top of the buildup. Omnes et al. (1988) tested offset VSP for imaging of the Springdale reef in Michigan. Meyer and Tittle (1998) used offset VSP to determine the correct position of a reef in East Texas. The target was represented by amplitude whitening in the offset VSP image. Ibrahim et al. (2010) interpreted high-resolution crosswell seismic data to examine the structure of the Niagaran reef in Michigan. In seismic images, the reef appeared as a low-amplitude region; the image "from below" presented more details from inside the reef body.

Since irregular reef edges scatter seismic energy, seismic diffractions may function as a complementary attribute for reef delineation. In this study, we evaluate the ability of seismic diffractions to supplement conventional techniques oriented to reefal buildup mapping. We interpret subsurface reef covered by carbonate sediments in the Volga Region of Russia. This reefal body had been revealed by drilling. To define its margins, we use VSP data obtained from six source stations placed around the borehole at different azimuths and almost equal offsets. We extract diffractions from VSP data and construct diffraction images for each acquisition azimuth. We perform multicomponent analysis for each discovered diffraction event to detect diffracted wave arrival directions and locate scattering sources. The located diffractors outline the reefal body. For reef delineation, the diffractions are used together with sections of instantaneous amplitudes.

GEOLOGICAL BACKGROUND

The geological structure of the study area in the Volga Region of Russia is composed of formations of Archean-Proterozoic ages, which form the crystalline basement, and a sedimentary sequence of Paleozoic-Mesozoic ages. Peterson and Clarke (1983) discussed the following main sedimentation cycles in this area. Riphean and Vendian stages are associated with shales and sandstones. These Proterozoic formations are overlain by Middle Devonian-Tournaisian transgressive deposits. These deposits include sandstone, siltstone, and shale, followed by carbonates and abundant reefs, and range up to 1000 m in thickness. The next Visean-Namurian-Bashkirian cycle begins with clastic deposits, which wrap around the reefs, and are overlain by marine carbonate beds. The Lower Moscovian-Lower Permian cycle consists of 1000 to 3000 m of terrigenous clastic deposits and marine carbonate beds. Evaporite deposits followed by marine limestones and dolomites compose the upper Lower Permian-Upper Permian cycle.

The main objective of our study - the reefal buildup - is related to the Famennian time (of the Upper Devonian); seismic facies of organogenic buildups are observed in the whole range of deposits, from early to late

Famennian. Surface seismic interpretation indicates that, because of reef building, most of the fields discovered in the study area are associated with zones of increased thickness in the range of time related to Frasnian-Famennian deposits. Structures that drape over the reefs act as traps and form hydrocarbon deposits in sediments including the Tournaisian, Bobrikovsky, Oka, and Bashkir.

VSP DATA ACQUISITION AND PREPROCESSING

The VSP data acquisition geometry is illustrated in Fig. 1. The data were acquired from six vibrator stations located around the borehole at different azimuths and at offsets of about 1500 m. The vibrator sweeps had a beginning frequency of 16 Hz and an end frequency of 110 Hz. One zero-offset source station was used for velocity estimation.

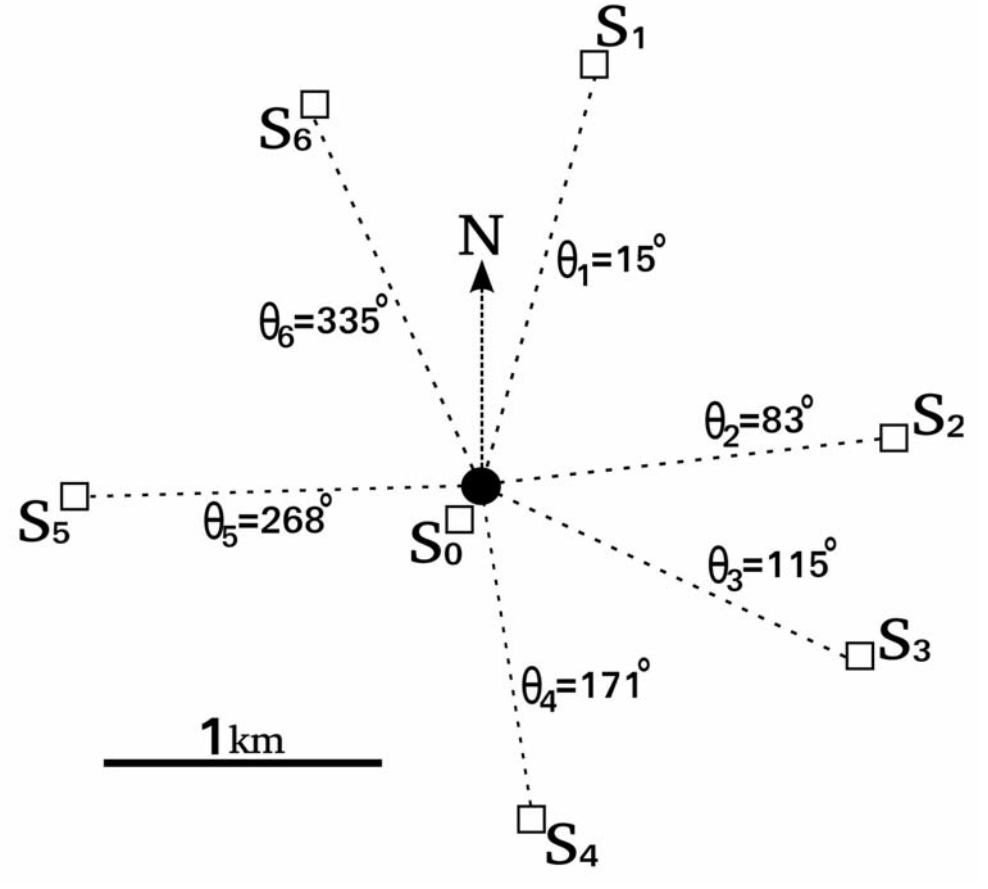

Fig. 1. Acquisition geometry. The borehole is the black dot. Source locations are represented by the squares.

Three-component data were recorded at 189 levels. The receivers were deployed at a depth interval from 120 to 3880 m, with a spacing of 20 m. The record length was 4 s with a 1 ms sample rate.

The VSP data preprocessing was performed using the following procedures. First, the three recorded geophone components were rotated to get the compressional component aligned toward the source, the radial component parallel to the "source-borehole" plane, and the transverse component orthogonal to this plane. Then, geometrical spreading was compensated. The wavefield was preliminarily separated into downgoing and upgoing components by f-k filter. The downgoing wavefield was used for signal shape estimation followed by deconvolution. Finally, the upgoing component was separated from the deconvolved wavefield.

ATTRIBUTE ANALYSIS

Before working with diffractions, we applied analysis of instantaneous amplitudes, a conventional technique for reef detection. As input, we used sections obtained after the vertical seismic profiling-common depth point (VSP-CDP) mapping (Dillon and Thomson, 1984; Wiggins et al., 1986). This transformation allows reflection boundaries to be imaged with minimal distortion of amplitudes.

The instantaneous amplitude sections (the compressional component) for each acquisition azimuth are presented in Figs. 2-4. We combined sections that are almost along the same line. The attribute reveals horizontal bedding; one strong reflection boundary outstays at a depth of 2.5 km.

The object of interest is deposited in the interval between 3.0 and 3.4 km. The reef may be detected by the perceptible amplitude weakening. The instantaneous amplitudes allow estimation of the body size and its orientation. The "dim spot", which we associate with the reef, extends 0.2 km away from the well in azimuth 1; however, its lateral extent cannot be traced in azimuth 4 (Fig. 2). In other azimuth directions, the body is stretched to 0.4 km away from the well (Figs. 3 and 4). Thus, the reef appears to be oblong, with a width of about 0.8 km and extending along azimuth 4.

DIFFRACTION IMAGING

To separate diffractions and construct diffraction images, we used an approach previously applied by Klokov et al. (2014). First, we attenuated reflections. The horizontal bedding leads to almost parallel reflection events in gathers. Estimation of the slope of these events followed by directional filtering

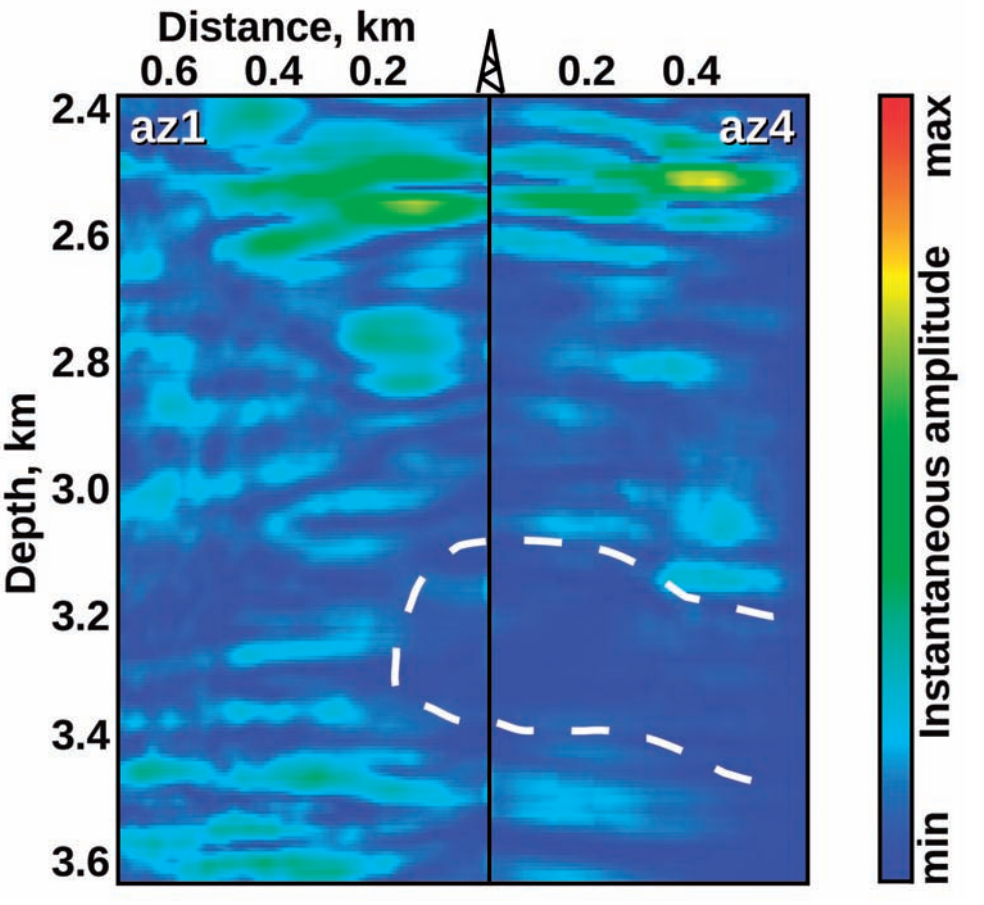

Fig. 2. Instantaneous amplitudes (the compressional component) for azimuth 1 and azimuth 4. The white dash outline indicates the "dim spot" associated with the reef. "azN" means the azimuth to source station N.

allowed us to eliminate reflections with high accuracy. Second, the residual "no-reflections" data were migrated into the dip-angle domain (Koren and Ravve, 2011). In this domain, diffraction events appear flat if the migrated gather matches the scatterer location and become sloped at the position away from the scatterer (Klokov and Fomel, 2012). This geometrical feature allowed the separation of diffractions from different kinds of noise that corrupted the residual data. We performed the separation using the Radon Transform. Finally, stacking of the separated diffraction events produced a diffraction image. This workflow was performed separately for each acquisition azimuth and each VSP data component.

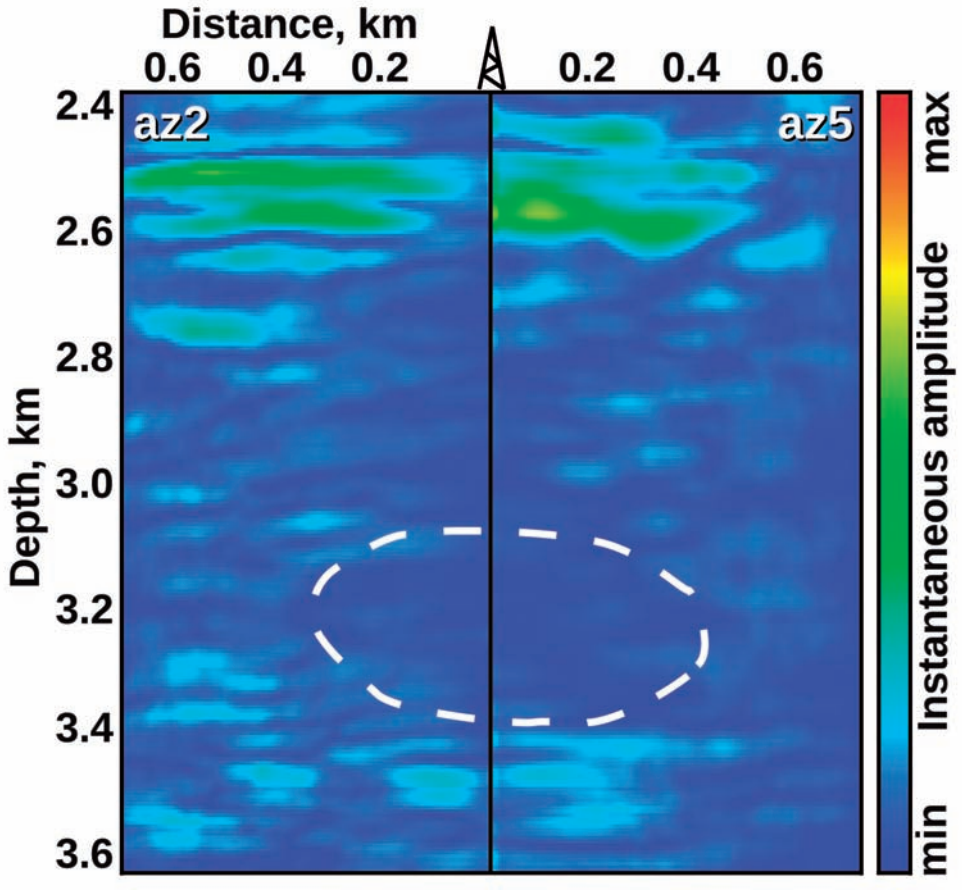

Fig. 3. Instantaneous amplitudes (the compressional component) for azimuth 2 and azimuth 5. The white dash outline indicates the "dim spot" associated with the reef. "azN" means the azimuth to source station N.

Diffraction images for each source are shown in Figs. 5 and 6. In this work, we mostly address the radial component, because this VSP data component appeared to be most sensitive to seismic diffractions and stable with respect to noise (Klokov et al., 2014). One diffraction image for the transverse component as well as one conventional migrated image for the radial component are displayed for reference. The seismic sections are tied to the well-based velocity profile and gamma log.

Strong correlation exists among the diffraction images from different sources and also between diffraction images and borehole logging. The interval

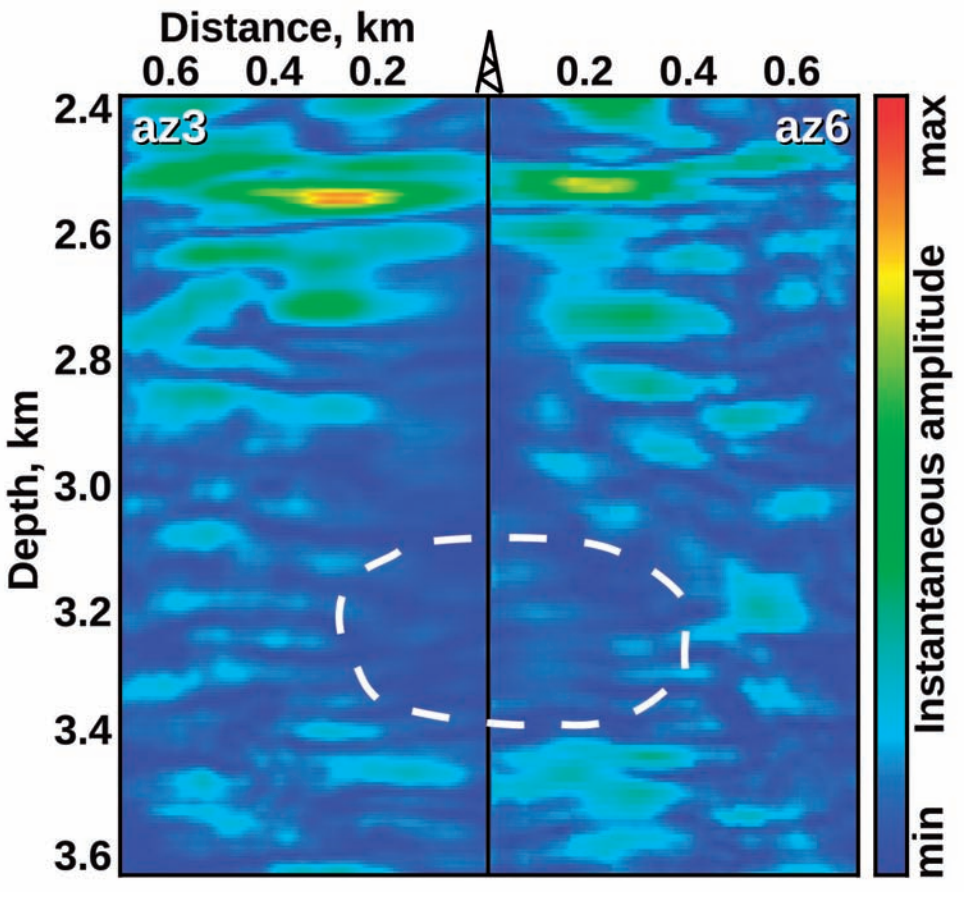

Fig. 4. Instantaneous amplitudes (the compressional component) for azimuth 3 and azimuth 6. The white dash outline indicates the "dim spot" associated with the reef. "azN" means the azimuth to source station N.

of the reef (2.8-3.3 km) has the highest velocities and lowest gamma values, which indicates pure compacted carbonate rock. In the diffraction images, this interval looks quiet - it contains only a few separated scatterers, which probably correspond to reef edges. Note that the scatterers are imaged as oblique strokes because of the VSP acquisition geometry (Keho, 1984). The covering interval of 2.6-2.8 km is supposed to be composed of carbonate, as well. However, velocities decrease and the diffraction sections reveal denser scatterer distribution, which may be associated with less compacted rock. The interval of 2.5-2.6 km is the Bobrikovsky horizon, whose lower part is composed of argillites and upper part is composed of oil- and water-saturated sandstones.

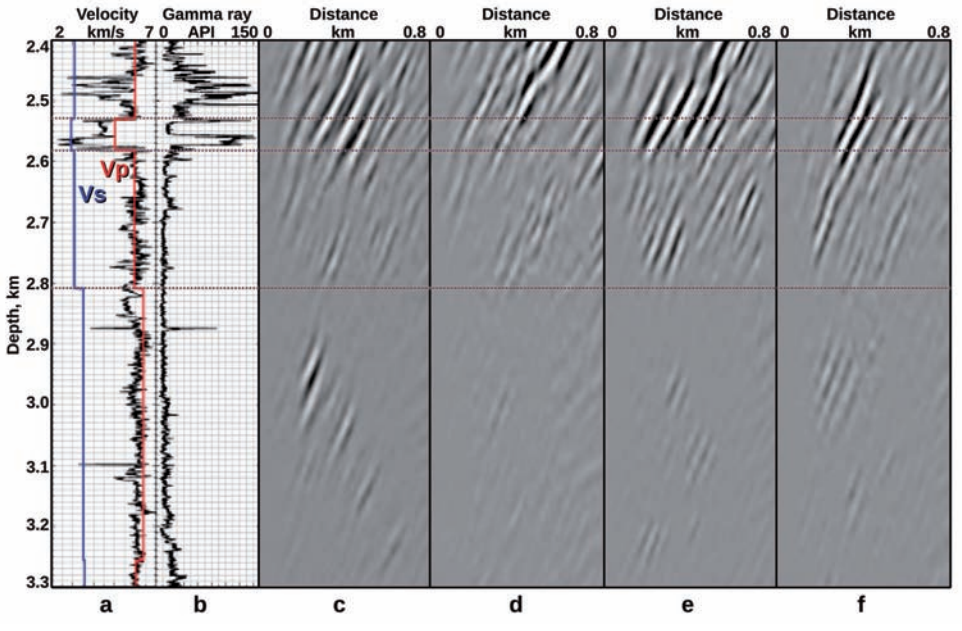

Fig. 5. Diffraction images tied to velocity profile and gamma log. (a) Interval velocities (solid lines) for compressional and shear waves. Acoustic log is plotted in black. (b) Gamma log. (c) Diffraction image for the radial component for source 1. (d) Diffraction image for the radial component for source 2. (e) Diffraction image for the radial component for source 3. (f) Diffraction image for the transverse component for source 3.

Diffractions in this interval are stronger than those in the underlying layers, a fact probably associated with variations in fluid saturation, which can create significant impedance contrasts. This feature was previously observed in other borehole and described by Klokov et al. (2014). The upper interval of 2.4-2.5 km is composed of many small saturated layers that yield strong diffractivity, as well.

One problem that arises when working with 2D surveys, such as offset VSP, is out-of-plane objects. Some scatterers may be removed from the plane "source-borehole", but printed at the imaging plane in incorrect positions (Biondi, 2006; Hobbs et al., 2006). Therefore, diffractors imaged in Figs. 5 and 6 only indicate the presence of diffraction sources in the vicinity of the image line. To be used for reef margins delineation, these objects should be located at the proper positions.

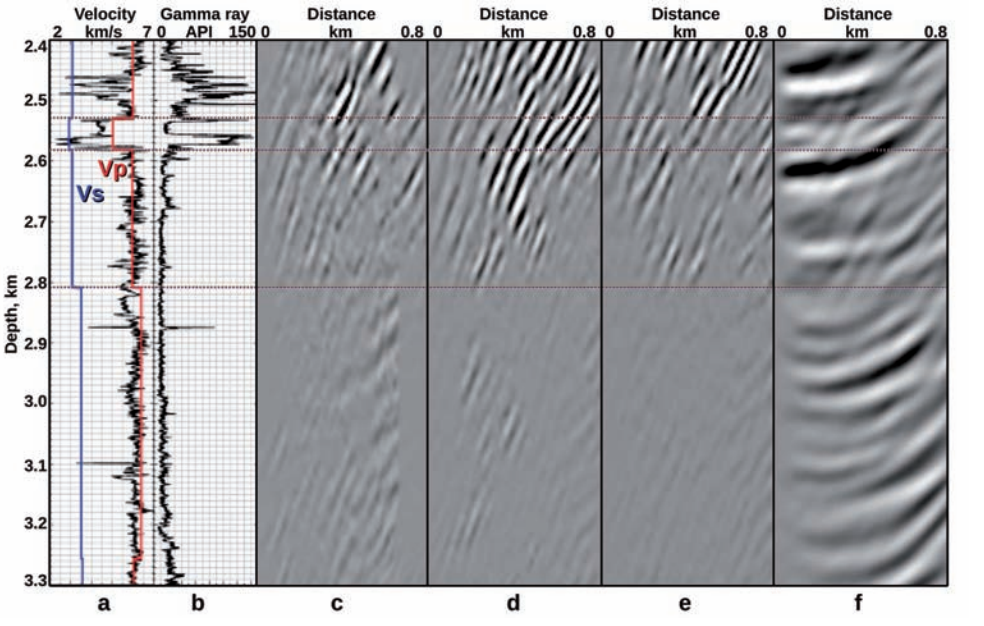

Fig. 6. Diffraction images tied to velocity profile and gamma log. (a) Interval velocities (solid lines) for compressional and shear waves. Acoustic log is plotted in black. (b) Gamma log. (c) Diffraction image for the radial component for source 4. (d) Diffraction image for the radial component for source 5. (e) Diffraction image for the radial component for source 6. (f) Conventional image for the radial component for source 6.

LOCATING DIFFRACTORS

Arrivals of diffracted waves are generally registered by all components of borehole sensors. Joint amplitude analysis of diffraction events at all three data components allows estimating the azimuth of arrival of diffracted waves and locating the diffraction sources. Humphries (2009) performed this kind of analysis to locate diffractions originating from faults.

To define the outlines of the reef, we first re-rotated our VSP data obtained after reflection elimination. We made one component vertical, one horizontal component parallel to the plane "source-borehole", and the second horizontal component orthogonal to this plane. Then, we ran 3D migration for each no-reflections gather and built azimuthal images around the borehole. Sections obtained after 2D imaging (Figs. 5 and 6) were taken to be corresponding to the zero azimuth. Each scattering object detected in diffraction

images (Figs. 5 and 6) was imaged in each azimuthal section. Generally, with azimuth increase, the scatterer was shifting upward and toward the borehole. We traced each scatterer along the azimuthal sections and tested each possible position of the object: we calculated a diffraction curve, took amplitudes from each data component along this curve, and estimated arrival azimuth. For the azimuth estimation, we used the approach based on the solution of the eigenproblem for the covariance matrix (Kanasewich, 1981). Consistency between tested scatterer azimuth and estimated azimuth was chosen as the imaging condition. Rectilinearity, which is a measure of wave linear polarization and varies between 0 and 1, was used as an additional criterion for quality control - all scatterers providing rectilinearity less than 0.5 were rejected as not reliable.

Fig. 7 displays a diffraction image for source 1 and three components of data from source 1 taken after reflection elimination and residual data re-rotation. Scatterers detected in the image and corresponding diffraction curves are marked by the same numbers. Note that the data still contain a large amount of noise; however, the diffraction events are traced with confidence, which may be used as an additional argument for the validation of the objects. Thus, events 4, 6, 7, and 8 are traced very well at each data component. Event 9 appears strong at the horizontal components but is corrupted at the vertical component. Events 2 and 5 look to be valid. All the diffraction curves - including curve 1, which appears to not fit any event - provide high values of rectilinearity, which is a quality control test. Note that scatterer 1 is weak, so its event is probably masked by noise. Event 3 is well traced at the H1-component but distorted at the H2-component. Multicomponent amplitude analysis of such event may cause an error. As confirmation, event 3 provided low rectilinearity value and was therefore excluded from the reef contour. (In total, we removed 3 of 37 points analyzed).

The noise interferes with arrival azimuth estimations. However, we did not perform any additional filtering to preserve diffraction amplitudes. Instead, to reduce the effect of noise, we limited the number of analyzed traces. The outlines in Fig. 7 identify traces that were used for the azimuth detection.

The scatterer locating was consistently performed for each acquisition azimuth. The detected positions of scatterers are collected in Figs. 8a and 8b, which are perspective view and map view, respectively. Diffractors are displayed in color to identify the acquisition azimuth from which they were detected. Diffractors illuminated by source 1 (shown in red) are marked by the numbers, as discussed above in Fig. 7.

Diffractors are generally located on both sides of the "source-borehole" plane, but some of them are significantly removed. Note that scatterers 5, 6, 8, and 9 are detected by two different azimuths - there are two close-located points

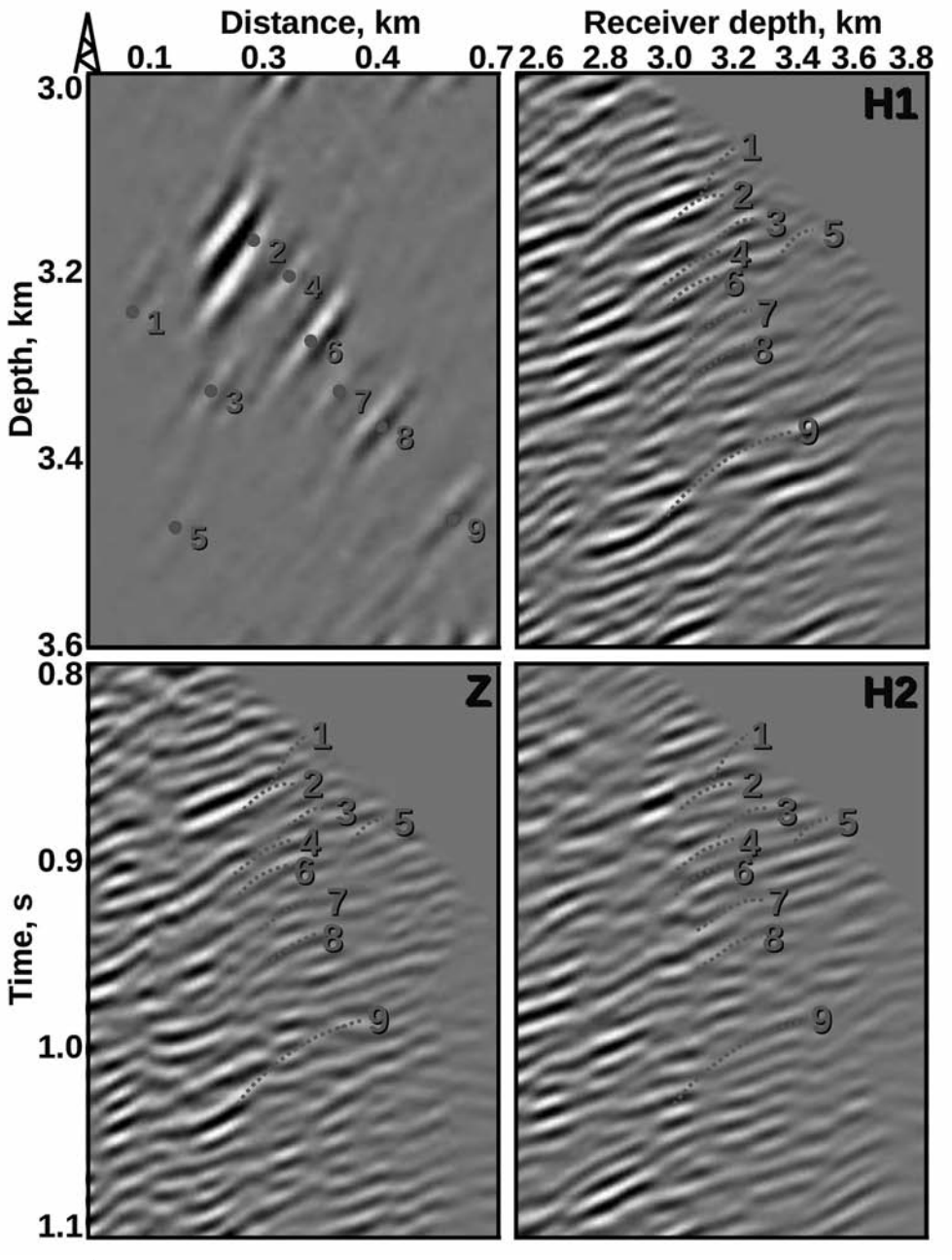

Fig. 7. Diffraction image for the radial component from azimuth 1 (top left) and three data components from azimuth 1 after reflection elimination and data re-rotation. Detected scatterers and corresponding diffraction curves are marked by the same numbers.

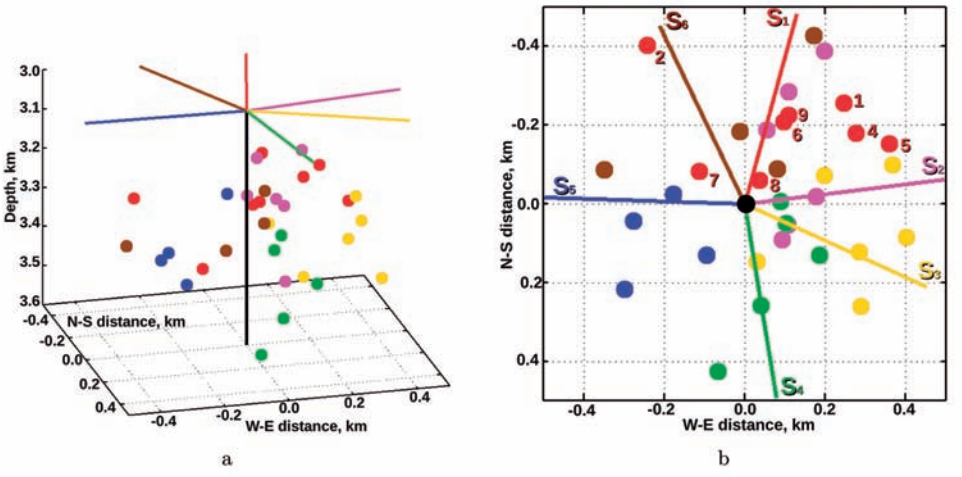

Fig. 8. Scatterers located around the borehole: (a) perspective view, and (b) map view. The scatterers are displayed in the same color as the acquisition azimuth from which they were detected. The vertical black line denotes the borehole.

of different colors - that can be used for validation of the reef edges. The positioning misfit may be explained by the inaccuracy of the velocity model used for migration, as well as the fact that the polarization analysis was complicated by data noise. At the same time, points 1, 2, 4, and 7 look isolated. The possible reason is that diffraction events corresponding to these scatterers might be obstructed by noise at other acquisition azimuths, or the events might be damaged by data preprocessing. Either problem would not allow imaging of the scatterers and locating their positions. Another possible reason is angular variations in scattering power (Liu et al., 1997), which is associated with the shape of the edge and with the arrival direction of the incident wave. Note that point 3 was not plotted because it did not pass the rectilinearity test.

The detected scatterers are distributed around the borehole at a distance not exceeding 0.4 km, which corresponds to the reef dimensions estimated from the attribute analysis. Along azimuth 1, scatterers are observed at a distance of about 0.2 km, which also fits the corresponding instantaneous amplitude section. The points are located closer to the well at shallower depths that infers a the domed-shape for the body. Note that diffractors are mostly concentrated north of the well, which is consistent with the assumption about the reef extension along azimuth 4 (shown in green). Thus, diffractions confirm conclusions made after seismic attributes interpretation and provide extra information from the space between acquisition azimuths.

DISCUSSION AND CONCLUSIONS

Seismic waves scattered by reef edges and registered by borehole sensors reveal power sufficient enough to be detected and used for delineation of reef margins. We were able to trace diffraction events at all three recorded VSP data components, to perform polarization analysis, and to define the arrival direction of diffracted waves, thereby detecting the position of scattering objects. The collection of located scatterers outlined the reefal body.

Diffractions confirmed interpretation of instantaneous amplitude sections. It is worth noting that we used two different kinds of input data. Instantaneous amplitudes were calculated for the product of VSP-CDP mapping, an analysis in the transformed data domain. Diffractions, in turn, were investigated in the image domain, after Kirchhoff migration. The consistency between these two interpretation approaches reinforces the conclusions made about the reef dimensions.

We observed that some of the scatterers were illuminated by different source stations, which validates the detected objects. At the same time, some diffraction points did not have counterparts; the scatterers were imaged by single sources. We explain this by the relatively high noise levels occur in some gathers, as well as by suboptimal preprocessing procedures that could destroy diffraction events. Scattering objects might also not be illuminated equally from different azimuths because of angular variations of scattering power.

Diffraction waves demonstrate the capability to complement conventional VSP data interpretation workflows. Diffractions recorded by multicomponent borehole sensors allow a multiazimuth view around a borehole. Multicomponent diffraction analysis may be particularly effective for interpretation of salt domes, which have high scattering features because of high impedance contrast with surrounding sediments.

ACKNOWLEDGMENTS

We thank Valentina Bogdanova and Bob Hardage for their support and motivating discussions.

REFERENCES

Adriansyah, A. and McMechan, G., 2001. AVA analysis and interpretation of a carbonate reservoir: Northwest Java basin, Indonesia. Geophysics, 66: 744-754.

Anderson, N., Brown, R., Hinds, R. and Hills, L., 1989. Seismic signature of a Swan Hills (Frasnian) reef reservoir, Snipe Lake, Alberta. Geophysics, 54: 148-157.

Antonelli, M., Miranda, F., Terzi, L. and Valenti, G., 2004. Integrated crosswell seismic: Case histories in advanced technologies to improve reservoir description. First Break, 22: 56-49.

Biondi, B.L., 2006. 3D Seismic Imaging. Investigations in Geophysics Series No. 14. SEG, Tulsa, OK. 224 pp.

Bueno, J., Honrio, B., Kuroda, M., Vidal, A. and Pereira Leite, E., 2014. Structural and stratigraphic feature delineation and facies distribution using seismic attributes and well log analysis applied to a Brazilian carbonate field. Interpretation, 2: SA83-SA92.

Caughlin, W., Lucia, F. and McIver, N., 1976. The detection and development of Silurian reefs in northern Michigan. Geophysics, 41: 646-658.

Chopra, S., and Marfurt, K.J., 2007. Seismic attributes for prospect identification and reservoir characterization. SEG and EAGE, Geophysical Developments No. 11, 464 pp.

Chuanmao, L. and Friedman, G.M., 1992. Petrophysical analysis of modern reef rocks: Carbonates and Evaporites, 7: 11-20.

Dillon, P.B. and Thomson, R.C., 1984. Offset source VSP surveys and their image reconstruction. Geophys. Prosp., 32: 790-811.

Dupal, L. and Miller, D.E., 1985. Reef delineation by multiple offset borehole seismic profiles: A case study. Expanded Abstr., 55th Ann. Internat. SEG Mtg., Washingon D.C.: 105-107.

Hardage, B.A., 2000. Vertical Seismic Profiling: Principles. Pergamon Press, Handbook of Geophysical Exploration, Vol. 14, 572 pp.

Hobbs, R.W., Drummond, B.J. and Goleby, B.R., 2006. The effects of three-dimensional structure on two-dimensional images of crustal seismic sections and on the interpretation of shear zone morphology. Geophys. J. Internat., 164: 490-500.

Humphries, M., 2009. Locating VSP diffracted arrivals using a microseismic approach. Expanded Abstr. 79th Ann. Internat. SEG Mtg., Houston: 4184-4188.

Ibrahim, M., Pennington, W. and Turpening, R., 2010. Crosswell seismic imaging of acoustic and shear impedance in a Michigan reef. The Leading Edge, 29: 706-711.

Kanasewich, E.R., 1981. Time Sequence Analysis in Geophysics. The University of Alberta Press, 480 pp.

Keho, T.H., 1984. Kirchhoff migration for vertical seismic profiles. Expanded Abstr., 54th Ann. Internat. SEG Mtg., Atlanta: 694-696.

Klokov, A. and Fomel, S., 2012. Separation and imaging of seismic diffractions using migrated dip-angle gathers. Geophysics, 77: S131-S143.

Klokov, A., Irkabaev, D., Ogiesoba, O., Skachek, K. and Munasypov, N., 2014. Diffraction analysis for the Sortym Formation using vertical seismic profiling data. J. Seismic Explor., 23: 463-480.

Koren, Z., and Ravve, I., 2011. Full-azimuth subsurface angle domain wavefield decomposition and imaging, Part I: Directional and reflection image gathers. Geophysics, 76: S1-S13.

Kuhme, A., 1987. Seismic interpretation of reefs. The Leading Edge, 6: 60-65.

Liu, E., Crampin, S. and Hudson, J., 1997. Diffraction of seismic waves by cracks with application to hydraulic fracturing. Geophysics, 62: 253-265.

Marroquin, I., Brault, J. and Hart, B., 2009. A visual data-mining methodology for seismic facies analysis: Part 2. Application to 3D seismic data. Geophysics, 74: P13-P23.

Meyer, J.H. and Tittle, W., 1998. Exploration risk reduction using borehole seismic: East Texas pinnacle reef applications. Expanded Abstr., 68th Ann. Internat. SEG Mtg., New Orleans: 369-372.

Omnes, G., Wu, C. and Turpening, R., 1988. Experimental reservoir delineation project in Michigan: Surface and borehole seismic images of the springdale reef. Expanded Abstr., 58th Ann. Internat. SEG Mtg., Anaheim: 165-167.

Peterson, J. and Clarke, J., 1983. Petroleum geology and resources of the Volga-Ural province, USSR. US Geological Survey Circular, 885, 27 pp.

Phipps, C.V.G. and Roberts, H.H., 1988. Seismic characteristics and accretion history of Halimeda biotherms on Kalukalukuang Bank, eastern Java Sea (Indonesia). Coral Reefs, 6: 149-159.

Russian, C., Perez, R., Marfurt, K., Davogustto, O., Alzahrani, H. and Small, A., 2010. P- and S-wave delineation of the Horseshoe Atoll, Diamond-M Field, Texas, USA. The Leading Edge, 29: 1108-1115.

Saadatinejad, M.R. and Sarkarinejad, K., 2011. Application of the spectral decomposition technique for characterizing reservoir extensional system in the Abadan Plain, southwestern Iran. Marine Petrol. Geol., 28: 1205-1217.

Skirius, C., Nissen, S., Haskell, N., Marfurt, K., Hadley, S., Ternes, D., Michel, K., Reglar, I., D'Amico, D., Deliencourt, F., Romero, T., D'Angelo, R. and Brown, B., 1999. 3-D seismic attributes applied to carbonates. The Leading Edge, 18: 384-393.

Verwer, K., Braaksma, H. and Kenter, J., 2008. Acoustic properties of carbonates: Effects of rock texture and implications for fluid substitution. Geophysics, 73: B51-B65.

Wiggins, W., Ng, P. and Manzur, A., 1986. The relation between the VSP-CDP transformation and VSP migration. Expanded Abstr., 56th Ann. Internat. SEG Mtg., Houston: 565-568.